Title

Multimodal Whole Brain Registration: MRI and High Resolution Histology

Permalink

https://escholarship.org/uc/item/50v7x8hf

ISBN

9781467388504

Authors

Alegro, Maryana
Amaro, Edson
Loring, Burlen
et al.

Publication Date

2016

DOI

10.1109/cvprw.2016.85

Copyright Information

Peer reviewed

Multimodal Whole Brain Registration: MRI and High Resolution Histology

Maryana Alegro
University of California San Francisco
maryana.alegro@ucsf.edu

Edson Amaro-Jr
University of São Paulo
eamaro@usp.br

Burlen Loring
Lawrence Berkeley National Laboratory
National Energy Research Scientific Computing
bloring@lbl.gov

Helmut Heinsen
University of Wüerzburg
University of São Paulo
heinsen@uni-wuerzburg.de

Eduardo Alho
University of São Paulo
eduardoalho@hotmail.com

Lilla Zöllei
Massachusetts General Hospital
lzollei@nmr.mgh.harvard.edu

Daniela Ushizima*
Lawrence Berkeley National Laboratory
University of California Berkeley
dushizima@lbl.gov

Lea T Grinberg*
University of California San Francisco
University of São Paulo
lea.grinberg@ucsf.edu

*authors contributed equally to this work

Abstract

Three-dimensional brain imaging through cutting-edge MRI technology allows assessment of physical and chemical tissue properties at sub-millimeter resolution. In order to improve brain understanding as part of diagnostic tasks using MRI images, other imaging modalities to obtain deep cerebral structures and cytoarchitectural boundaries have been investigated. Under availability of postmortem samples, the fusion of MRI to brain histology supports more accurate description of neuroanatomical structures since it preserves microscopic entities and reveal fine anatomical details, unavailable otherwise. Nonetheless, histological processing causes severe tissue deformation and loss of the brain original 3D conformation, preventing direct comparisons between MRI and histology. This paper proposes an interactive computational pipeline designed to register multimodal brain data and enable direct histology-MRI correlation. Our main contribution is to develop schemes for brain data fusion, distortion corrections, using appropriate diffeomorphic mappings to align the 3D histological and MRI volumes. We describe our pipeline and preliminary developments of scalable processing schemes for high-resolution images. Tests consider a postmortem human brain, and include qualitatively and quantitatively results, such as 3D visualizations and the Dice coefficient (DC) be-tween brain structures. Preliminary results show promising DC values when comparing our scheme results to manually labeled neuroanatomical regions defined by a neurosurgeon on MRI and histology data sets. DC was computed for the left caudade gyrus (LC), right hippocampus (RH) and lateral ventricles (LV).

1. Introduction

Cutting-edge MRI technology allows non-invasive acquisition of structural brain images with sub-millimeter resolution in clinical neuroscience [16]. However, modern scanners at maximum resolution still lack the average $1\mu m^3$, attained by conventional microscopy [14]. Therefore, histology continues to be the gold standard for brain anatomy, since MRI images are insufficient to support definition of cytoarchitectural boundaries and small inner brain regions [6]. Many studies attempt to correlate MRI signal to tissue features to enable brain assessment *in vivo* and deeper understanding of the nervous system. Precise MRI-histology correlation represents a breakthrough in exploring the neuronal basis of MRI signal [17], estimating neuroanatomical structures boundaries [5], investigating neuropathology disease mechanisms [18] and aiding the construction of histology based brain atlases [2], among others.

Direct MRI-histology comparison is precluded by artifacts inherent to histological processing. Brain tissue bears considerable local and global deformations caused by manipulation during procurement from skull and fixation. Serial sectioning often perforates and tears the tissue, and also compromises the original 3D geometry, for example, attempts to simply stack back the slides often yield deformed, twisted volumes, a phenomenon known as z-error [23]. Chemical processing, such as dehydratation and staining, causes shrinking and uneven shading. The combination of these artifacts lead to huge geometric differences between MRI and histology image sets [27], requiring the use of intricate non-linear deformation models for correction. Moreover, considerable contrast heterogeneity between MRI and histology makes registration more complex, requiring the calculation of robust similarity metrics [11]. These modalities also have different acquisition and sectioning planes, making direct alignment unfeasible. Moreover, full human brain histological processing yields hundreds of images, and processing this large data set can be computationally intensive [5].

Histology to MRI registration is emerging as a powerful, yet challenging task. Several authors investigate this problem applying linear and non-linear registration methods to tissue data from animals, such as mice [36, 4, 13] and monkey [14]. Studies using human tissue are scarce, given the difficulties in procuring and processing such material. Singh et al. [28] use high order polynomial mapping to register photographs of one human brain hemisphere to their approximate whole head MRI slices. Instead, Osechinskiy et al. [25] use thin-plate splines to register sparsely sectioned slides from a human brain hemisphere to a whole head MRI. Adler et al. [1, 2] use a graph-based registration method to register hippocampi tissue samples to their respective MRI volume. Registration studies using whole human brain histology are even more infrequent. To the best of this authors knowledge, only two studies handle the registration of whole human brain histology to MRI. Yang et al. [35] combine 3D affine registration and 2D non-linear section-to-section registration, but authors do not provide information about the specific method used for registering a whole human brain low-resolution histological volume to its counterpart MRI, while Amunts et al. [5] use 2D affine section-to-section registration and 3D diffeomorphic mapping to register a high-resolution whole brain histology to its MRI.

Here we propose an interactive computational pipeline designed to handle all the histology complexities and register histological samples to their counterpart MRI. The pipeline allows processing high-resolution histological whole brain images, aiming to preserve near-microscopic features. We describe our preliminary results running this pipeline on a large distributed memory system, required to deal with the data size. Finally, we estimate our proposed registration scheme through visualizations and calculation of Dice coefficients.

2. Materials and Methods

2.1. MRI and Histology Acquisition

This study uses a postmortem whole human brain donated to research upon a signed informed consent and IRB approval. The brain was scanned in-cranio (i.e. brain inside the skull, without any chemical treatment) ex-vivo (right after death) in a 3.0 T Philips Achieva MR scanner using an 8-channel head coil. We acquired conventional clinical T1-weighted Inversion-recovery 3D Fast Field Echo sequence (TR = 6,3ms; TE = 2,9 ms; TI = 791 ms; 240 x 240; $1mm^3$ voxels; slices oriented to the mid-sagittal plane) stored in DICOM format.

After MRI acquisition, the specimen was processed using a celloidin-embedding protocol [19, 32]. Briefly, the brain was fixed in 10% buffered formalin for several weeks, dehydrated in graded series of ethanol solutions, soaked in 8% celloidin solution and celloidin-mounted by means of a vacuum-assisted embedding procedure. The resulting block was serially sectioned on a sliding microtome (Polycut, Cambridge Instruments, UK) with section thickness of 400μm in the axial plane. The block was photographed during the serial sectioning, before each microtome stroke, using a Canon 5D Mark III camera and 50mm AutoMakro Olympus lens attached to a copystand (these images were called "blockface"). The camera was carefully placed over the block to avoid motion during the sectioning process and to enforce constant distance between block and sensor, thus yielding images that were perfectly aligned within the data set. This procedure also ensured that each histological slice has a counterpart blockface image.

All sections were stained using a modified gallocyanin (Nissl) technique optimized for highlighting neuronal bodies [19] and mounted on glass slides. Each stained slide was place over a portable light table with uniform white backlight and imaged using a Fuji Finepix II camera and a 50mm AutoMakro Olympus lens attached to the copystand. All pictures were taken with the same magnification and distance from the camera, assuring a standard scale through the whole set. Rulers were placed near the tissue to allow calculation of the true pixel resolution. The whole data set spanned 279 images, each with 0.02x0.02x0.4mm voxel resolution, stored in JPEG format. Figure 1 shows examples of the histology, blockface and MRI. The celloidin-embedding method reduces the overall amount of artifacts and prevents occurrence of tears. Further details on embedding and staining protocols can be found in [19, 18].

Figure 1. Example of histological slice (left), blockface image (center) and MRI (right) as discussed in Sec. 2.

2.2. Pipeline description

Our core strategy for registering the 2D histological images to the 3D MRI volume includes: (1) to use the blockface as a template for properly positioning the slices within the histological data sets; (2) to create an intermediate 3D volume, and finally (3) to use a 3D registration algorithm to register histology to MRI. These three main steps include several image processing algorithms applied to the histology and MRI data in order to improve registration between these modalities. Figure 2 shows an outline of the proposed pipeline, and the following sections describe each pipeline step.

2.2.1   Histology pre-processing

Blockface and Histology Segmentation: Blockface images can be compressed by eliminating the unnecessary background. Any general purpose registration method, not based on landmarks, will consider the alignment of the entire histological image to the MRI, yielding inaccurate results. Thus, background segmentation is a critical pre-processing step. As part of our segmentation strategy, we use an orthogonal color model that allows pixels to cluster in specific regions in the colorspace, a computer vision algorithm also applied to human skin image segmentation [34]. This step transforms the blockface RGB images into the YIQ space, such as Y is a luminance component and I and Q are color components. Tissue pixels form clusters on the IQ space and are modeled as a Gaussian mixture model (GMM). We calculate two Gaussian distributions for modeling tissue and background. Expectation maximization (EM) is used for estimating the GMM parameters. As a default, EM is initialized by randomly assigning pixels to both classes. All image pixels are then classified using this model, yielding an initial brain binary mask. Finally, we use active contours [12] to further refine the mask. The resulting mask is essential to segment the tissue region and is stored for future processing. Users can, optionally, initialized the EM with pre-selected samples from tissue and background. This option often improves classification results for difficult images. Users can also disable the active contours refinement to speed-up processing at the cost of obtaining less accurate results.

The stained histology images are simpler than their counterpart blockfaces, being composed of large colored re-

gions over mostly empty background. However, they still need to be segmented since this background may contain dirt, bubbles and other undesired findings. Similarly to the blockface images, histology tissue pixels also cluster in specific regions of the IQ space, so we extend the method from the earlier to later.

All segmented images are converted to grayscale using the transformation in 1, where x is a image intensity for R,G and B, the red, green and blue channels, respectively.

$$G(x) = 0.2989R(x) + 0.5870G(x) + 0.1140B(x) \quad (1)$$

All our input images are JPEG and output images are saved as Nifti for it is a more suitable format for the next processing steps. This segmentation method was implemented in Matlab.

2D registration: The blockface data set preserves information about correct slice positioning within the histological image volume and is used as a template for correctly aligning those images. Our strategy is to register each histological image to its corresponding blockface and stack them, thus creating a histology volume free of z-effect. The blockface, however, bears deformations caused by brain removal and fixation, therefore unreliable to recover the brain original shape.

Histology to blockface registration is performed using an affine model and Mattes mutual information similarity [24], which is tailored to handle multi-modality registration problems. Histological images are registered independently. All transform matrices are stored for future use. We particularly use ANTs [9] affine registration implementation in this step.

Intensity correction and stacking: Intensity inconsistency is a common artifact among histology slices caused by different lighting conditions during imaging and variations in staining concentrations. It causes a stripping effect orthogonal to the sectioning plane that can interfere with visualization and analysis of anatomical structures and may result in registration errors. We employ an iterative global histogram matching scheme [22] for intensity correction. It is performed after 2D registration to correct any global intensity change that may be introduced during the previous step. All enhanced images are stacked to form an intermediate 3D volume. This step was fully implemented in Matlab.

Sampling: Processing the histological images at their full resolution involves registrations that require memory footprint larger than the 128GB available in our system nodes. Due to this limitation, we sample the histology volume to a lower resolution. We empirically found that $0.15mm^3$ is the maximum resolution we could process, given our computational pipeline. We used ITK cubic-spline interpolation for downsampling the data set.

Next, the user manually initializes the data set orientation matrix by roughly aligning the histology to MRI through the FreeSurfer's Freeview tool that computes an
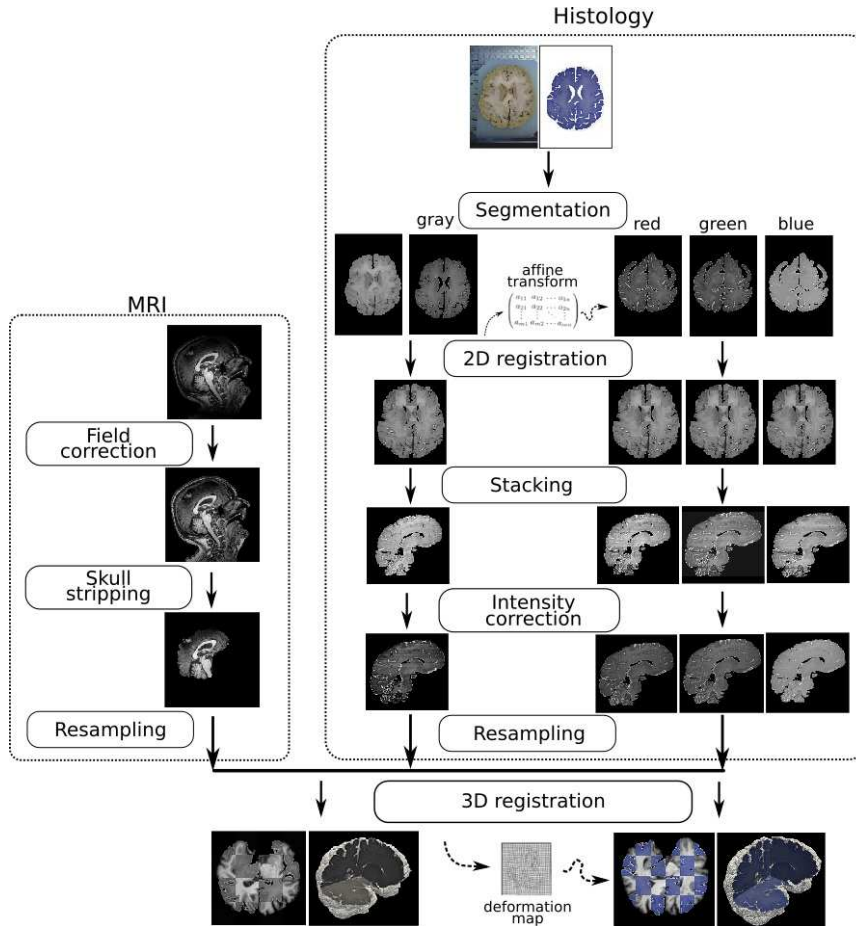
Figure 2. Diagram of the proposed pipeline, with two main independent tasks: MRI processing and histology processing.

affine transform matrix. This step is necessary to create an initial overlap between data sets, allowing the registration algorithm to work properly. Notice that this is the only mandatory user intervention.

2.2.2 MRI Pre-processing

Field inhomogeneity correction: Since field intensity heterogeneity may reduce the overall processing quality, we include the N3 algorithm [29], as a correction step to minimize spurious variations.

Skull stripping: Any general purpose registration method not using landmarks will register the histology to the MRI as whole and will not consider only the brain tissue. Thus, skull segmentation is a critical step. All structures not belonging to the brain must be removed otherwise the final registration will be distorted. We used FSL brain extraction tool (BET) tool [30] in our pipeline, which is a mature, well tested segmentation tool.

Sampling: Histology images have much higher resolution than their MRI counterpart, so registration includes down-sampling histological data, blurring out important boundary information and small inner brain structures, while still remaining the essential features to allow fusion between the modalities. We employ cubic spline sampling to bring the MRI to an intermediate resolution space, preventing excessive blurring of structures of interest during the registration process. This step was implemented in ITK.

2.2.3 3D Registration

We use diffeomorphic non-linear 3D registration for aligning the histological volume to its counterpart MRI, thus recovering most of its original shape and allowing direct comparison between both modalities. Diffeomorphisms are differentiable mapping with differentiable inverses. They are onto, meaning that all elements in the domain are mapped to elements in its range; and one-to-one, meaning that different elements in the domain can not mapped to the same element in the range. These properties guarantee that connected sets remain together, disjoint sets remain separate, coordinates are transformed in a consistent way and topol-

ogy is preserved. Thus, diffeomorphic registration ensures that all pixels in the registered image are mapped to all pixels in the fixed image, in a one-to-one way [10]. The diffeomorphic registration framework is robust in the presence of deformations and is suitable for registering data with complex intensity relationships.

This paper uses the symmetric diffeomorphic registration method (SyN) described by Avants et al. [7] due to its robustness to large deformations, symmetry property (i.e. the registration map is invertible, so the order of choice between target and movable images does not bias the registration) and accurate results in registering brain images, as in [20]. SyN models the transform function as a geodesic (shortest path) in the space of diffeomorphic mappings ϕ that connects I, the movable image (histology), and J, the target image (MRI). The forward mapping can be written as $\phi I = I(\phi(x, t = 1))$ and inverse mapping as $\phi_{-1}(x, 1)$. SyN splits the mapping in 2 equal length geodesics ϕ_1 and ϕ_2, so that ϕ_2 runs in opposite direction to ϕ_1, making I and J equally contribute to the registration mapping. The registration process minimizes the following objective function:

$$E_{cc}(\overline{I}, \overline{J}) = \inf_{\phi_1} \inf_{\phi_2} \int_{t=0}^{0.5} \{\|v_1(\mathbf{x}, t)\|_L^2 + \|v_2(\mathbf{x}, t)\|_L^2\} dt$$
$$+ \int_{\Omega} CC(\overline{I}, \overline{J}, \mathbf{x}) d\Omega \quad (2)$$

Such that ϕ_i in the solution for the ordinary differential equation $\frac{d\phi_i(\mathbf{x},t)}{dt} = v_i(\phi_i(\mathbf{x}, t), t)$. Here $\mathbf{x}$ is a spatial coordinate, t time, v_1 and v_2 are square-integrable, continuous vector fields that represent the velocity of traversing ϕ_i (v_i is an approximately arc length parametrization, that guarantees all ϕ_i are of the same length), $\|.\|_L$ is a regularization term that smooths the velocity field and $CC(\overline{I}, \overline{J}, \mathbf{x})$ stands for the cross-correlation computed using sliding windows over I and J. The first term in the objective function introduces enough smoothness on the vector field to force the resulting map to be diffeomorphic. The second term measures the similarity between mapped and target image. The vector field is computed using the Euler-Lagrange equations derived from 2 and an iterative optimization method described in [8]. The original formulation uses cross-correlation as the similarity metric; however, the diffeomorphic framework allows the use of other metrics for driving the registration.

We use the ANTs toolbox [9] SyN implementation as part of our pipeline. We superseded the cross-correlation with Mattes mutual information (MI) [24]. We chose MI after tests with methods using local similarity measures, such as DRAMMS [26] and SyN using CC, yield poor registration results with our data. All input volume is in Nifti format, however we use Nrrd file for format as output. This format is particularly convenient for visualization as is can be read in parallel by the visualization tool. The mappings

(ϕ_i) computed by SyN are saved and stored for later use in color reconstruction.

2.2.4 Color Reconstruction and Scalable Visualization

Staining plays an important role in histology analysis as it is used to identify specific cytoarchitectural features, chemical components (i.e proteins), acidity levels and other attributes. However, most registration studies in literature do not include color in their final results. Furthermore, most medical image viewers do not allow visualization of color volumes or limit this functionality for specific aims, such as displaying fMRI LUTs or pseudo-color PET scans. Most medical image viewers are also not designed to be scalable, failing to load and manage big data sets.

We design a color reconstruction step in our pipeline to allow inspection of histology original colors. In this step, all original histological images are split in red, green and blue channels. Each channel is registered to its corresponding blockface by applying the affine transform previously computed during the 2D Registration. Each channel of each histological image is then stacked, corrected for intensity inconsistency and resampled as described in the previous sections, yielding a red, green and blue image volume. Each channel volume is registered to the MRI by applying the diffeomorpic maps computed during the 3D registration. Finally, the registered channels are combined to form the registered color volume. This process is depicted in Figure 2, where intermediate processing results for each color channel can be seen in the right part.

We perform visualization (volume rendering) of the registered grayscale and color volumes using ParaView, instead of a standard medical viewer for its scalability, as it is able to run on distributed memory computing resources thus handling large data sets.

3. Results

All MRI processing and histology/blockface segmentation calculations ran on a standard workstation (Intel(R) Xeon(R) 6-core CPU 2.40GHz E5-2620, 16GB RAM). All the remaining histology processing steps (see Figure 2) executed in one node (Intel(R) Xeon(R) 32-core CPU 2.30GHz E5-2698, 128GB RAM) of a large shared memory system. ParaView server ran on the same system using 24 nodes. The upsampled MRI and pre-registration histology data sets were stored in 8 bits, yielding about 9 Gigabytes (GB) each. However, both datasets had to be converted to double precision during the registration process, yielding a 23GBs volume, each. The final registered grayscale and red, green and blue volumes presented 23 GBs, each. All data sets had their intensities rescaled and were converted back to 8 bits due to storage constraints.

The proposed pipeline processed the whole brain and the registration result was evaluated qualitatively and quantitatively. Visual inspection of the volume rendering revealed appropriate registration quality, according to the neurologists in charge. Figure 3 shows a checkerboard visualization of the histology overlaid on the MRI, Figure 6 emphasizes the 3D reconstruction for comparison with the MRI volume and Figure 5 renders three different planes for further details. Inspection of the checkerboard views and 3D volumes reveals coherence on the deformations. White matter and gray matter boundaries are consistently matched, so are the gyri on most of the images. Registration errors are visible, especially in the inner brain region. This is also visible in Figure 3a, where the left hippocampus shows a large difference when compared to the right hippocampus. The volume rendering also allows to assess that our registered histology is capable of resolving inner brain structures not visible on the original and resampled MRIs, as shown in Figure 6: the red nucleus boundaries are visible in histology (a), while very fuzzy on the resampled (c) and original (d) MRIs. Intensity correction errors are visible near the cerebellum in Figure 5 and (b).

Quantitative evaluation was performed by computing the Dice coefficient (DC):

$$DC = \frac{2|A \cap B|}{|A| + |B|}$$

between stacks of masks manually labeled on the MRI and original histology data sets. A and B are two sets of binary masks and $|.|$ is the set cardinality. DC captures how precise is the localization between A and B, which is computed quickly and with straightforward interpretation. An experienced neurosurgeon segmented the left caudate gyrus (LC), right hippocampus (RH) and lateral ventricles (LV) on the MRI images and on the original histology images (these regions were selected because they have well-defined boundaries on the MRI). The histology segmentations were registered using the affine transforms pre-computed during the 2D registration and mapped to the MRI using the diffeomorphic maps computed during the 3D registration. Finally, they were thresholded into a binary set. Figure 4 shows a 3D reconstruction of the stacked binary masks. DC was computed between MRI and registered masks sets for the selected structures. RH DC was 0.59, LV DC was 0.65 and LC DC was 0.75.

4. Discussion

This paper proposed an interactive computational pipeline for registering high-resolution whole human brain histological images and described our preliminary results. It was tested with images of a whole brain and assessed registration quality by visualization and quantification through Dice coefficient.
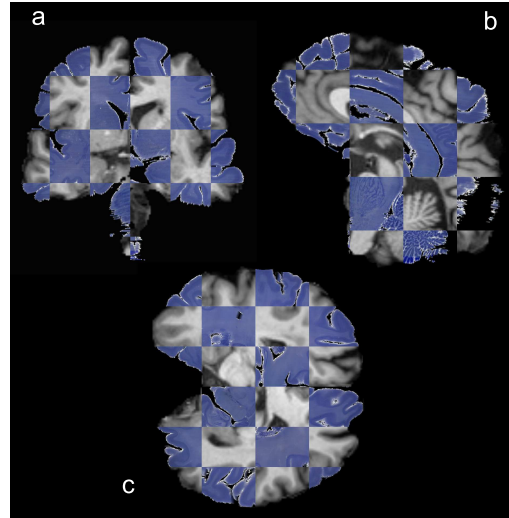

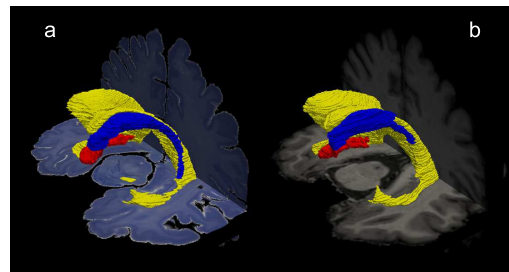Figure 3. Registered histology overlaid on MRI images.

Figure 4. 3D reconstruction of the stacked binary masks. a) histology binary masks after registration; b) MRI binary masks. The right hippocampus (red), left caudade nucleus (blue) and lateral ventricles (yellow) can be seen in both images.

Our ultimate goal is to be able to register and visualize the histology in its full resolution of 0.02x0.02x0.4mm. However, our first prototype can only register images up to $0.x15mm^3$, given that this is the highest resolution our tools support without running out of memory, even though we used a system with big memory nodes (128 Gigabyte RAM). The reason is that SyN, as well as most of the large deformation diffeormorphic metric mappings methods, stores big vector fields in memory thus having a large memory footprint [33]. Furthermore, these methods were not designed to scale up to a GB, so it does not take advantage of distributed memory systems. Henceforth, we aimed to find what was highest attainable resolution running ANTs toolbox without any modification. Despite some loss in resolution, our registered histology showed enhanced structures, otherwise not well resolved in MRI. Figure 6 emphasizes the case: the inner brain structures in (a), such as the red nucleus, have sharp boundaries, which are fuzzy in the MRI (b and c). We are aware that the MRI resampling
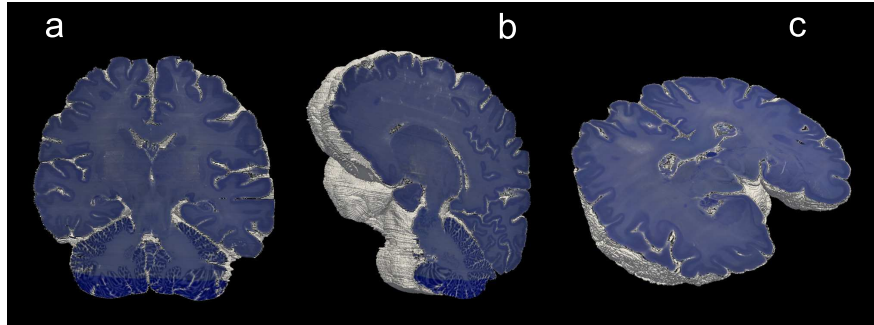
Figure 5. Histology 3D reconstruction using ParaView ($0.15mm^3$ resolution). a) coronal plane; b) sagittal; c) axial plane.
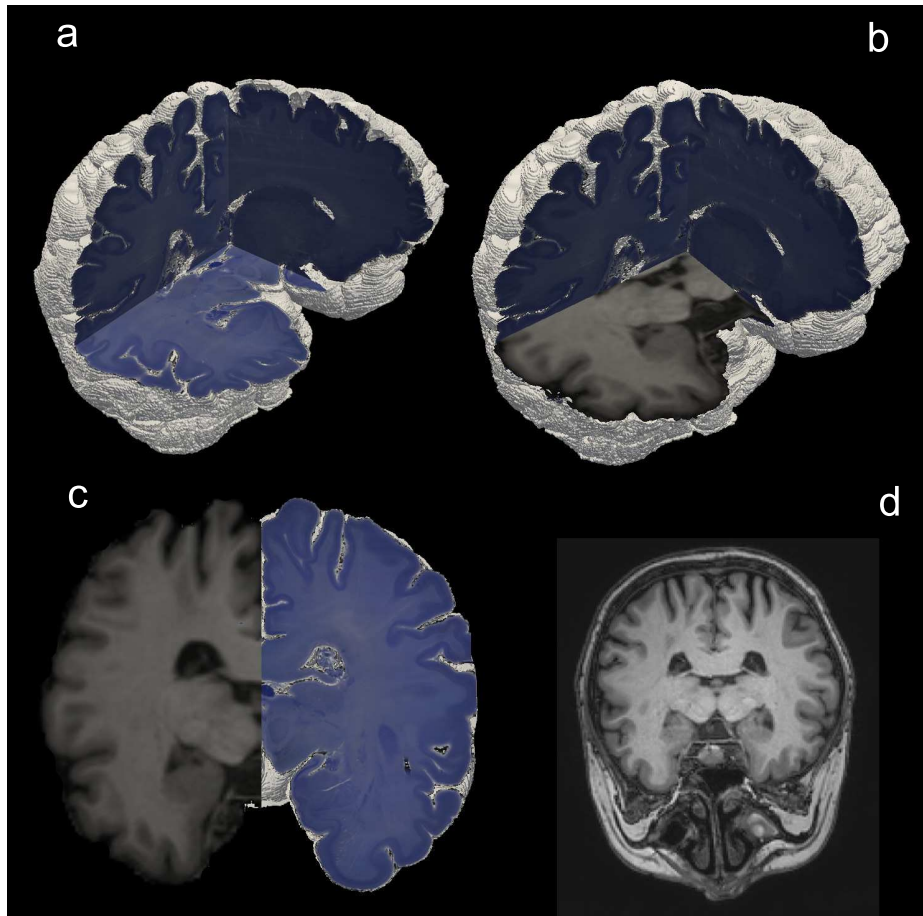

Figure 6. Histology 3D reconstruction using ParaView and visualization of the brain inner structures with $0.15mm^3$. a) Histology reconstruction; b) Corresponding MRI reconstruction for comparison. c) Axial view of the histology side-by-side with MRI; d) Original MRI slice located in the same region displayed in c.

causes loss of details, however notice that the MRI image did not present this structure in the raw data at all. We included the original MRI slide (Figure 6d) of that particular region for comparison.

We obtained Dice coefficients of 0.59 for right hippocampus, 0.65 lateral ventricles and 0.75 for left caudate gyrus. DC indicated the localization between two sets, however there is no fixed standard for an "accurate" value. Some authors consider DCs greater than 0.6 appropriate for small brain structures and 0.8 accurate for big ones [15, 31]. Other authors consider values above 0.7 as appropriate for localization in general purpose comparisons [3]. Our pre-

liminary results were sub-optimal if considering these values as standards, probably due to poor initial centralization. Manual centering of the histology volume was a burdensome (given the site of the high-resolution data set) and often inaccurate task that requires visual inspection. DC, nonetheless, does not give accurate information regarding shape and also, our analysis was biased towards few inner brain structures. Improvements on quantification of the registration quality will include more brain regions as well as shape metrics, such as [21], that can assess brain structures geometry.

We performed visualization of the registered grayscale and color volumes using ParaView. We chose this tool instead of a standard for medical viewer for its scalability, as it is able to run on distributed memory computing resources and to handle extreme large data sets. ParaView is also very versatile allowing visualization of color images, surfaces, 2D and 3D objects in the same scene. To the best of our knowledge, this is the first time a whole brain high-resolution histology visualization is performed using a massive parallel scientific visualization tool. By using ParaView we were able to visualize the color high-resolution histology overlaid on MRI, as well as the grayscale volumes and also pseudo-color representations.

Our preliminary results are promising since we were ultimately able to register a whole human brain histology volume to its counterpart MRI, with resolution higher than what a modern MRI scanner can acquire in clinical practice. We were able to render inner brain structures, otherwise unresolved in standard clinical MRI in a scalable fashion, by using a non-specific scientific visualization tool. Future work will address full resolution histology, including new registration methods that are capable of scaling to take advantage of distributed memory systems, an automatic method for centralization of the histology volumes and inclusion of different imaging modalities, such as PET.

Acknowledgments

References

[1] D. H. Adler, A. Y. Liu, J. Pluta, S. Kadivar, S. Orozco, H. Wang, J. C. Gee, B. B. Avants, and P. A. Yushkevish. Reconstruction of the human hippocampus in 3d from histology and high-resolution ex-vivo mri. *IEEE International Symposium on Biomedical Imaging*, 2012. 2

[2] D. H. Adler, J. Pluta, S. Kadivar, C. Craige, J. C. Gee, B. Avants, and P. A. Yushkevish. Histology-derived volumetric annotation of the human hippocampal subfields in postmorten mri. *NeuroImage*, 84, 2014. 1, 2

[3] A. Akbarzadeh, D. Gutierrez, A. Baskin, M. R. Ay, A. Ahmadian, N. R. Alam, K. O. Loevblad, and H. Zaidi. Evaluation of whole-body mr to ct deformable image registration. *Journal of Applied Clinical Medical Physics*, 14, 2013. 7

[4] L. Alic, J. C. Haeck, S. Klein, K. Bol, S. R. van Tiel, P. A. Wielepolski, M. Bijster, W. J. Niessen, M. Bernsen, J. F. Veenland, and M. Jong. Multi-modal image registration: matching mri with histology. *SPIE*, 7626, 2010. 2

[5] K. Amunts, C. Lepage, L. Borgeat, H. Mohlberg, T. Dickscheid, M. Rousseau, S. Bludau, P. Bazin, L. Lewis, A. Oros-Peusquens, N. Shah, T. Lippert, K. Zilles, and A. Evans. Bigbrain: an ultrahigh-resolution 3d human brain model. *Science*, 340(6139), 2013. 1, 2

[6] J. Annese. The importance of combining mri and large-scale digital histology in neuroimaging studies of brain connectivity and disease. *Frontiers in Neuroinformatics*, 6(13), 2002. 1

[7] B. B. Avants, C. L. Epstein, M. Grossman, and J. C. Gee. Symmetric diffeomorphic image registration with cross-correlation: Evaluating automated labeling of elderly and neurodegenerative brain. *Medical Image Analysis*, 12, 2008. 5

[8] B. B. Avants, P. T. Schoenemann, and J. C. Gee. Lagrangian frame diffeomorphic image registration: Morphometric comparison of human and chimpanzee cortex. *Medical Image Analysis*, 2005. 5

[9] B. B. Avants, N. Tustison, and G. Song. Advanced normalization tools (stnava.github.io/ants). March 2015. 3, 5

[10] M. F. Beg, M. I. Miller, A. Trouve, and L. Younes. Computing large deformation metric mapping via geodesic flows of diffeomorphisms. *International Journal of Computer Vision*, 61(2), 2005. 5

[11] C. Ceritoglu, L. Wang, L. D. Selemon, J. G. Csernansky, M. I. Miller, and J. T. Ratnanather. Large deformation diffeomorphic metric mapping registration of reconstructed 3d histological section images and in vivo mr images. *Frontiers in Human Neuroscience*, 43(4), 2010. 2

[12] T. Chan and L. A. Vese. Active contours without edges. *IEEE Transactions on Image Processing*, 10(2), 2001. 3

[13] A. Cifor, L. Bai, and A. Pitiot. Smoothness-guided 3d reconstructioin of 2d histological images. *NeuroImage*, 56, 2011. 2

[14] J. Dauguet, T. Delzescaux, F. Condé, J. F. Margin, N. Ayache, P. Hantraye, and V. Frouin. Three-dimensional reconstructions of stained histological slices and 3d non-linear registration with in-vivo mri for whole baboon brain. *Journal of Neuroscience Methods*, 164, 2007. 1, 2

[15] B. Dawant, S. Hartmann, J. P. Thirion, F. Maes, D. Vandermeulen, and P. Demaerel. Automatic 3d segmentation of internal structures of the head in mr images using a combination of similarity and free-form transformation part ii: methodology and validation on severely atrophied brains. *IEEE Transactions on Medical Imaging*, 18, 1999. 7

[16] J. H. Duyn. The future of ultra-high field mri and fmri for study of the human brain. *NeuroImage*, 62(2), 2012. 1

[17] S. Eickhoff, N. Walters, A. Schleicher, J. Kril, G. Egan, K. Zilles, J. Watson, and K. Amunts. High-resolution mri reflects myeloarchitecture and cytoarchitecture of human cerebral cortex. *Human Brain Mapping*, 24(3), 2005. 1

[18] L. Grinberg, E. Amaro-Jr, A. Silva, R. Silva, J. Sato, D. Santos, S. Pacheco, R. Lucena, R. Leite, C. Pasqualucci, S. Teipel, W. Flatz, and H. Heinsen. Improved detection of incipient vascular changes by a biotechnological platform combining post mortem mri in situ with neuropathology. *Journal of the Neurological Sciences*, 283(2), 2009. 1, 2

[19] H. Heinsen, T. Arzberger, and C. Schmit. Celloidin mounting (embedding without infiltration) - a new, simple and reliable method for producing serial sections of high thickness through complete human brains and its application to stereological and immunohistochemical investigations. *Journal of Chemical Neuroanatomy*, 20(49), 2000. 2

[20] A. Klein, J. Andersson, B. A. Ardekani, J. Ashburner, B. B. Avants, M. C. Chiang, G. E. Christensen, D. L. Collins, J. Gee, P. Hellier, J. H. Song, M. Jenkinson, C. Lepage, D. Rueckert, P. Thompson, T. Vercauteren, R. P. Woods, J. J. Mann, and R. V. Parsey. Evaluation of 14 nonlinear deformation algorithms applied to human brain mri registration. *NeuroImage*, 1(46), 2009. 5

[21] E. Konukoglu, B. Glocker, A. Criminisi, and K. M. Pohl. Wesd - weighted spectral distance for measuring shape dissimilarity. *IEEE Transactions on Patterns Analysis and Machine Intelligence*, 35(9):2284–2297, September 2013. 8

[22] G. Malandain and E. Bardinet. Intensity compensation within series of images. In *MICCAI 2003*, LNCS, 2003. 3

[23] G. Malandain, E. Bardinet, K. Nelissen, and W. Vanduffel. Fusion of autoradiographs with an mr volume using 2-d and 3-d linear transformations. *NeuroImage*, 23:111, 2004. 2

[24] D. Mattes, D. R. Haynor, H. Vesselle, T. K. Lewellen, and W. Eubank. Pet-ct image registration in the chest using free-form deformations. *IEEE Transactions on Medical Imaging*, 22(1), 2003. 3, 5

[25] S. Osenchinskiy and F. Kruggel. Slice-to-volume nonrigid registration of histological sections to mr images of the human brain. *Anatomy Research International*, 2011, 2011. 2

[26] Y. Ou, A. Sotiras, N. Paragios, and C. Davatzikosa. Dramms: Deformable registration via attribute matching and mutual-saliency weighting. *Medical Image Analysis*, 15:622, 2011. 5

[27] A. Pitiot and A. Guimond. Geometrical regularization of displacement fields for histological image registration. *Medical Image Analysis*, 12:16, 2008. 2

[28] M. Singh, A. Rajagopalan, C. Zarow, X. L. Zhang, T. S. Kim, D. Hwang, A. Y. Lee, and H. Chui. From human mri to microscopy: co-registration of human brain images to post-morten histological sections. *IEEE Medical Imaging Conference*, 2006. 2

[29] J. G. Sled, A. P. Zijdenbos, and A. C. Evans. A non-parametric method for automatic correction of intensity non-uniformity in mri data. *IEEE Transactions on Medical Imaging*, 18, 1998. 4

[30] S. M. Smith. Fast robust automated brain extraction. *Human Brain Mapping*, 2002. 4

[31] B. Sparks, S. Friedman, D. Shaw, E. Aylward, D. Echerlard, A. Artru, K. Maravilla, J. Giedd, J. Munson, G. Dawson, and S. Dager. Brain structural abnormalities in young children with autism spectrum disorder. *Neurology*, 59, 2002. 7

[32] P. Theofilas, L. Polichiso, X. Wang, L. Lima, A. T. L. Alho, R. E. P. Leite, C. K. Suemoto, C. A. Pasqualucci, W. Jacob-Filho, H. Heinsen, and L. T. Grinberg. Brazilian aging brain study g. a novel approach for integrative studies on neurodegenerative diseases in human brains. *Journal of Neuroscience Methods*, 226, 2014. 2

[33] T. Vercauteren, X. Pennec, A. Perchant, and N. Ayache. Symmetric log-domain diffeomorphic registration: A demons-based approach. *MICCAI*, 5241, 2008. 6

[34] J. Yang, W. Lu, and A. Waibel. Skin color modeling and adaptation. In *Computer Vision — ACCV'98*, volume 1352, pages 687–694, 1997. 3

[35] S. Yang, Z. Yang, K. Fischer, K. Zhong, J. Stadler, F. Godenschweger, J. Steiner, H. J. Heinze, H. G. Bernstein, B. Bogerts, C. Mawrin, D. C. Reutens, O. Speck, and M. Walter. Integration on ultra-high field mri and histology for connectome based research of brain disorders. *Frontiers in Neuroanatomy*, 7, 2013. 2

[36] P. A. Yushkevish, B. B. Avants, L. Ng, M. Hawrylycz, P. D. Burstein, H. Zhang, and J. C. Gee. 3d mouse brain reconstruction from histology using o coarse-to-fine approach. *WBIR*, 2006. 2